



## RESEARCH ARTICLE

# Changes in white matter functional networks during wakefulness and sleep

Yang Yang<sup>1,2</sup> | Shilei Wang<sup>1,2</sup> | Jiayi Liu<sup>1,2</sup> | Guangyuan Zou<sup>1,2</sup> | Jun Jiang<sup>1,2</sup> | Binghu Jiang<sup>3</sup>  | Wentian Cao<sup>2</sup> | Qihong Zou<sup>1,4</sup> 

<sup>1</sup>Center for MRI Research, Academy for Advanced Interdisciplinary Studies, Peking University, Beijing, China

<sup>2</sup>Beijing City Key Lab for Medical Physics and Engineering, Institution of Heavy Ion Physics, School of Physics, Peking University, Beijing, China

<sup>3</sup>Department of Radiology, Nanchong Central Hospital, The Second Clinical Medical College, North Sichuan Medical College, Nanchong, China

<sup>4</sup>National Clinical Research Center for Mental Health, Peking University Sixth Hospital, China

## Correspondence

Qihong Zou, Center for MRI Research, Peking University, 5 Yiheyuan Road, Haidian District, Beijing, China 100871.

Email: [zouqihong@pku.edu.cn](mailto:zouqihong@pku.edu.cn)

## Funding information

Beijing Municipal Science and Technology Commission, Grant/Award Number: Z181100001518005; Beijing United Imaging Research Institute of Intelligent Imaging Foundation, Grant/Award Number: CRIBJZD202101; National Key Research and Development Program of China, Grant/Award Number: 2018YFC2000603; National Natural Science Foundation of China, Grant/Award Numbers: 81671765, 81871427; Sichuan Science and Technology Program, Grant/Award Number: 2021JDRC0038

## Abstract

Blood oxygenation level-dependent (BOLD) signals in the white matter (WM) have been demonstrated to encode neural activities by showing structure-specific temporal correlations during resting-state and task-specific imaging of fiber pathways with various degrees of correlations in strength and time delay. Previous neuroimaging studies have shown state-dependent functional connectivity and regional amplitude of signal fluctuations in brain gray matter across wakefulness and nonrapid eye movement (NREM) sleep cycles. However, the functional characteristics of WM during sleep remain unknown. Using simultaneous electroencephalography and functional magnetic resonance imaging data during wakefulness and NREM sleep collected from 66 healthy participants, we constructed 10 stable WM functional networks using clustering analysis. Functional connectivity between these WM functional networks and regional amplitude of WM signal fluctuations across multiple low-frequency bands were evaluated. In general, decreased WM functional connectivity between superficial and middle layer WM functional networks was observed from wakefulness to sleep. In addition, functional connectivity between the deep and cerebellar networks was higher during light sleep and lower during both wakefulness and deep sleep. The regional fluctuation amplitude was always higher during light sleep and lower during deep sleep. Importantly, slow-wave activity during deep sleep negatively correlated with functional connectivity between WM functional networks but positively correlated with fluctuation strength in the WM. These observations provide direct physiological evidence that neural activities in the WM are modulated by the sleep-wake cycle. This study provided the initial mapping of functional changes in WM during sleep.

## KEYWORDS

EEG, fluctuation amplitude, fMRI, functional connectivity, NREM sleep, white matter functional networks

Yang Yang and Shilei Wang contributed equally to this study.

This is an open access article under the terms of the [Creative Commons Attribution-NonCommercial-NoDerivs](https://creativecommons.org/licenses/by-nc-nd/4.0/) License, which permits use and distribution in any medium, provided the original work is properly cited, the use is non-commercial and no modifications or adaptations are made.

© 2022 The Authors. *Human Brain Mapping* published by Wiley Periodicals LLC.

## 1 | INTRODUCTION

Functional magnetic resonance imaging (fMRI) has been widely used to study the brain function of healthy populations (Chaarani et al., 2021; Gordon et al., 2017) and the dysfunction associated with neurodegenerative diseases, such as Alzheimer's disease (Chen et al., 2021), Parkinson's disease (Wolters et al., 2019) and epilepsy (Hill et al., 2020; Li, Tavakol, et al., 2021). Due to its high sensitivity and noninvasiveness, the blood oxygenation level-dependent (BOLD) signal is the most commonly used contrast in fMRI research. However, in BOLD-fMRI studies, the detection of brain networks and local brain activity have mainly been focused on gray matter (GM) signals and cortical brain regions, and fMRI studies based on white matter (WM) signals remain largely misunderstood and overlooked (Grajauskas et al., 2019). Studies related to WM have been dedicated to investigating the structural architecture through structural imaging techniques, such as diffusion tensor imaging, that do not directly provide functional information regarding WM (Peer et al., 2017).

BOLD signals rely on cerebral blood flow (CBF) and cerebral blood volume (CBV); however, CBF and CBV in WM are much lower than those in GM (Helenius et al., 2003; Preibisch & Haase, 2001; Rostrup et al., 2000). Although detecting brain function using WM signals is controversial, reports of fMRI activation in WM are increasing (Gawryluk et al., 2014). Based on a visuomotor interhemispheric transfer task, a key report of WM fMRI activation was published by Tettamanti and colleagues, in which a cluster was observed in the genu of the corpus callosum (Tettamanti et al., 2002). Moreover, the findings of Tettamanti et al. were confirmed by other studies (Gawryluk et al., 2009; Omura et al., 2004; Weber et al., 2005). In addition to task studies, Ding et al. found that resting-state fMRI signals in WM exhibit anisotropic correlations (Ding et al., 2013). Recently, studies detecting brain function using WM signals have received increasing attention (Ding, Ding, et al., 2018; Ding, Huang, et al., 2018; Gore et al., 2019; Ji et al., 2019; Jiang, Luo, et al., 2019; Li et al., 2019; Li, Gao, et al., 2021; Peer et al., 2017). Peer and colleagues analyzed resting-state fMRI data from WM signals and demonstrated the existence of symmetrical WM functional networks that correlated with functional GM brain networks (Peer et al., 2017). Ding et al. showed that WM signals acquired from BOLD-fMRI reflected neural activities both in the resting state and during tasks (Ding, Huang, et al., 2018). Jiang and colleagues found changes in the perception-motor system in schizophrenia patients by detecting WM functional networks (Jiang, Luo, et al., 2019). These studies demonstrated that fluctuations in WM BOLD signals can reveal brain functional neural activities (Gore et al., 2019).

Sleep is the basic physiological state of humans and plays a very important role in maintaining human health and normal functions (Zhou et al., 2019). Nonrapid eye movement (NREM) sleep in humans includes light and deep sleep in repeating patterns of Stages 1, 2, and 3 (N1, N2, and N3). Each state is associated with specific GM functional connectivity patterns and frequency characteristics (Tagliazucchi et al., 2013). However, previous studies of sleep were mainly based on GM BOLD signals. To our knowledge, there have

been no studies evaluating brain activity using WM BOLD signals across the NREM sleep-wake cycle. Previous studies have found meaningful WM signals under resting-state conditions and during cognitive tasks related to neural activities. Whether functional connectivity and frequency characteristics of WM networks change in concordance with physiological transitions between wakefulness and NREM sleep needs to be investigated.

In this study, the differences in functional networks and regional characteristics of amplitude fluctuations across different physiological states (wakefulness and NREM stages) in healthy participants based on WM BOLD-fMRI signals were investigated. Clustering analysis was performed to obtain WM networks, and functional connectivity between each WM network was calculated. The amplitude of low-frequency fluctuations (ALFF) in each WM network across wakefulness and different sleep stages was calculated. The main effects of stage and post hoc analyses were used to compare the differences. To explore the physiological significance of WM functional connectivity and amplitude fluctuations, Pearson's correlations between WM brain activity during deep sleep and the power of slow-wave activity (SWA) were calculated. We hypothesized that individual differences in WM activity were influenced by sleep pressure, which was reflected in SWA during deep sleep.

## 2 | MATERIALS AND METHODS

### 2.1 | Participants

Seventy-three healthy participants (36 males and 37 females; age:  $27.76 \pm 8.67$  years old) were recruited from the campus of Peking University and the surrounding area of Beijing. These subjects were all right-handed, and none of them had the following conditions: (1) history of mental illness and neurological disease; (2) history of proven medical brain injury; (3) history of using psychotropic drugs; or (4) history of drug or alcohol abuse. All participants were required to avoid coffee and alcohol during the experiment. They provided written informed consent under the guidance of the experimenter and received monetary compensation for their participation. The study was approved by the Institutional Review Board of Peking University Sixth Hospital.

### 2.2 | Experimental design

The participants were required to maintain a regular schedule for 2 weeks before the electroencephalography (EEG)-fMRI experiment that was monitored by actigraphy and recorded in a sleep diary.

The experimental data were collected on an MRI scanner (3 T Prisma; Siemens Healthineers, Erlangen, Germany) at the Center of MRI Research, Peking University. Within 1 week after a 2-week period of sleep monitoring, each subject underwent an fMRI adaptation session. The subjects were asked to wear an EEG cap (64-channel, MR-compatible EEG system; Brain Products, Munich, Germany) lying in

the MRI scanner. The adaptation session included a 6-min T1-weighted scan and a 20-min BOLD-fMRI scan. Within 1 week after the adaptation scan, simultaneous EEG-fMRI data were acquired at the participant's usual bedtime when the participant had been instructed to sleep. It is worth noting that no sleep deprivation was involved.

### 2.3 | Data acquisition

During sleep, EEG-fMRI data were simultaneously acquired using a 3 T Prisma MRI Scanner and a 64-channel MR-compatible EEG system with a sampling rate of 5000 Hz. Based on the international 10/20 system, the 64-channel recording montage included 57 EEG channels, two electrooculography channels, two electromyography (EMG) channels, one electrocardiography (ECG) channel, and two reference channels (A1 and A2). The resistance of the reference and ground channels was reduced to less than 10 k $\Omega$ , and the resistance of other channels was kept below 20 k $\Omega$ . The resistance of 64 channels was checked before and after the fMRI scan to ensure the quality of EEG data. During the data acquisition process, sponge pads were used to limit the subjects' head movement, and earplugs were provided to reduce noise interference. Wires connecting the cap and the amplifiers were fixed to avoid any potential vibration during the MR scan. The EEG and fMRI data were synchronized in terms of triggers (SyncBox; Brain Products).

For registration purposes, high-resolution anatomical images of each subject were acquired by a 3D magnetization-prepared rapid gradient echo T1-weighted sequence (repetition time [TR] = 2530 ms; echo time [TE] = 2.98 ms; inversion time = 1100 ms; flip angle [FA] = 7°; number of slices = 192; matrix = 512  $\times$  448; and voxel resolution = 0.5  $\times$  0.5  $\times$  1.0 mm<sup>3</sup>). The participants were asked to keep their eyes closed and lie quietly in the scanner.

Then, the "sleep" session began after the participants were instructed to try and fall asleep. fMRI data were acquired using gradient echo-planar imaging (EPI) with the following parameters: TR = 2000 ms; TE = 30 ms; FA = 90°; number of slices = 33; slice thickness = 3.5 mm; gap = 0.7 mm; matrix = 64  $\times$  64; and in-plane resolution = 3.5  $\times$  3.5 mm<sup>2</sup>. Scanning ended when the largest number of volumes (4096 volumes for the EPI sequence in our scanner) was recorded or the participants were completely awake after sleeping and could not fall asleep again.

### 2.4 | EEG preprocessing and sleep stage scoring

EEG data preprocessing was implemented with BrainVision Analyzer 2.1 (Brain Products, Munich, Germany). The MR gradient artifacts in EEG data were eliminated by the average artifact subtraction method (Allen et al., 1998; Allen et al., 2000). For the ballistocardiogram artifacts, the R peaks were detected semiautomatically with manual adjustment for peaks misidentified by the software. The R peaks were transferred from the ECG to the EEG over a selectable time delay, and

the average artifacts were then subtracted from the EEG data (Allen et al., 2000). Next, the data were downsampled to 500 Hz, rereferenced to the mean values of channels A1 and A2, and temporally filtered (10–100 Hz for EMG channels and 0.3–35 Hz for the other channels) (Zou et al., 2021).

The sleep stages were scored for every 30-s frame of preprocessed EEG data and were performed visually by an experienced technician and double-checked by another experienced technician in accordance with American Academy of Sleep Medicine criteria (Iber et al., 2007). Sleep recordings were divided into five stages, including wakefulness (W), NREM stage 1 (Stage N1), NREM stage 2 (Stage N2), NREM stage 3 (Stage N3), and rapid eye movement sleep.

### 2.5 | fMRI data processing

fMRI data of continuous 5-min epochs of wakefulness, N1, N2, and N3 were extracted (Zou et al., 2021). It was shown that using a 5-min period of data was sufficient to estimate stable correlation strengths (Van Dijk et al., 2009). For each session, fMRI data were preprocessed using SPM8 ([www.fil.ion.ucl.ac.uk/spm](http://www.fil.ion.ucl.ac.uk/spm)), DPARSFA (Yan & Zang, 2010), and in-house MATLAB (MathWorks) scripts. As described in the original study by Peer and colleagues (Peer et al., 2017), the entire preprocessing steps of fMRI included the following: (1) Slice-timing correction. (2) Motion correction to the mean functional images using trilinear interpolation with 6 degrees of freedom. Subjects with maximum motion >2 mm or 2° were excluded from subsequent analysis, resulting in 11 sessions excluded. Sixty-six of the 73 participants (31 males and 35 females; age: 28.15  $\pm$  8.99 years old) were included in further analysis. (3) Removal of linear trends for signal drift correction. (4) Nuisance signal regression that included 24 head-motion-related regressors derived by Volterra expansion (Friston et al., 1996) and the mean cerebrospinal fluid (CSF) signals. (5) Filtering with a 0.01–0.15 Hz bandpass filter to limit non-neuronal contributions to BOLD fluctuations. (6) Scrubbing using motion "spikes" (framewise displacement >1 mm). (7) Spatial smoothing. To avoid mixing the signals of WM and GM, signals from GM and WM were separately smoothed (4-mm full-width half-maximum, isotropic) based on the respective masks of each participant. (8) Normalization to the standard EPI template and resampling to 3  $\times$  3  $\times$  3 mm<sup>3</sup> voxels using the DARTEL algorithm (Ashburner, 2007).

### 2.6 | Clustering analysis to obtain WM networks

Based on the above segmentation results, a tissue probability map of WM, GM, and CSF of each participant was obtained. To generate individual WM masks, tissue segmentation results of anatomical images from each individual were thresholded at 0.5. WM masks at the group level were generated as follows. If a voxel was recognized as WM in more than 60% of the participants, then this voxel was labeled WM in the group-level mask. Using existing segmentation methods, some

deep regions were easily classified as WM. The thalamus, caudate nucleus, putamen, globus pallidus and nucleus accumbens defined by the Harvard-Oxford Atlas were excluded from the group-level WM mask (Peer et al., 2017).

After obtaining the group-level WM mask, WM spatial networks were identified by a clustering algorithm. To reduce computational complexity in the subsequent cluster analysis, the WM mask was spatially downsampled based on an interchanging grid strategy (Peer et al., 2017), resulting in 4561 voxels in the subsampled WM mask. A whole-WM correlation coefficient matrix ( $18,278 \times 4561$ ) was obtained by calculating Pearson's correlation coefficients between each voxel in the WM mask and each voxel in the downsampled WM mask. The correlation coefficient matrices were averaged across the participants to obtain a group-level correlation coefficient matrix.

The K-means clustering method (distance metric-correlation, 10 replicates) was applied to the group-level correlation coefficient matrix to obtain WM functional networks, within which all the voxels had similar connectivity patterns with the rest of the voxels in the WM mask (Blumensath et al., 2013; Craddock et al., 2012; Moreno-Dominguez et al., 2014; Peer et al., 2014; Yeo et al., 2011). To determine the most stable number of WM networks, clustering analyses were performed with the number of clusters ( $K$ ) ranging between 2 and 22 (Lange et al., 2004; Yeo et al., 2011). The method to calculate the spatial stability of the clustering results corresponding to each  $K$  was as follows: (1) The correlation coefficient matrix was randomly divided into four folds along the columns. (2) For each  $K$ , clustering analysis was performed on the four folds of data separately. Relatively similar clustering results would be obtained if the stability was high (Lange et al., 2004; Yeo et al., 2011). The clustering results obtained by the clustering analysis were randomly labeled, so it was difficult to compare the similarity of cluster results based on the labels directly. To evaluate the similarity of the clustering results, the adjacent matrix was calculated for each clustering result from each fold. Then, the Dice coefficient was calculated to compare these adjacent matrices. For each  $K$ , all four adjacent matrices were compared in pairs. The mean value of the Dice coefficients was calculated to determine the number of clusters with high stability through the local peak point in the Dice coefficient graph (Peer et al., 2017).

## 2.7 | Functional connectivity between WM networks

Based on the multiple WM networks obtained by the above clustering analysis, the mean fMRI time courses within each WM network were extracted during each physiological state for each subject. Then, Pearson's correlation coefficients between each pair of WM networks was calculated and transformed to Fisher's  $z$  score ( $zFC$ ) for statistical analysis. The  $zFC$  data from the four stages were compared using the program 3dLMEr (Chen et al., 2013) in AFNI (Cox, 1996) and Bonferroni corrected ( $p < 10^{-16}$  corrected). WM network pairs with significant differences in FC across the four stages were obtained. Post hoc  $t$ -tests between paired networks were then conducted on

the basis of these significant differences to reveal which sleep states showed significant differences in FC.

## 2.8 | Frequency characteristics of WM networks

Spontaneous low-frequency oscillations in BOLD signals in the resting state are considered meaningful physiological indicators to study spontaneous brain activity (Fox & Raichle, 2007). Studies have shown that low-frequency bands can be divided into multiple subbands, and these different subbands may be associated with different physiological functions (Cha et al., 2016; Duan et al., 2017; Palva & Palva, 2012; Zuo et al., 2010). ALFF was adopted to capture the amplitude fluctuations of the WM signals. Consistent with a previous study on WM signals, ALFF over the 0.01–0.08 Hz band (Zang et al., 2006) for the WM network in each physiological state was calculated. The main effect of stage was performed on amplitude fluctuations from four physiological states using 3dLMEr and corrected with Bonferroni correction ( $p < 10^{-16}$ ). Post hoc analyses were then conducted to explore which sleep states were significantly different from each other.

In addition, the low-frequency band (0.01–0.08 Hz) was divided into two subbands based on a previous definition, namely, slow-5 (0.01–0.027 Hz) and slow-4 (0.027–0.073 Hz), to calculate the average fluctuation amplitude in slow-5 and slow-4 between different sleep states (Zuo et al., 2010). ALFF in these two subbands from four sleep states was calculated. The interaction effect between stage by frequency subband and the main effects of stage and frequency subband on ALFF were evaluated using 3dLMEr and corrected with Bonferroni correction ( $p < .001$ ).

## 2.9 | Slow-wave activity correlated with functional connectivity and frequency characteristics

The power spectral density was acquired using a fast Fourier transform on 5-min EEG data with artifacts removed based on a 4-s Hanning window and 2-s overlap, which was implemented by Welch's method based on a custom script ("pwelch" function in MATLAB 2017a). Then, SWA was computed, whose frequency band ranged from 0.75 to 4 Hz (Ly et al., 2016). To explore whether FC in these WM network pairs was electrophysiologically significant, Pearson's correlation coefficients between FC and SWA in N3 sleep was calculated. Similarly, the relationship between the fluctuation amplitude in the WM and SWA signal during N3 sleep was explored.

## 3 | RESULTS

### 3.1 | WM functional networks

Seventy-three sessions of wakefulness (16 males and 8 females; ages:  $27.46 \pm 8.11$  years old), 42 sessions of N1 sleep (12 males and 16 females; ages:  $27.32 \pm 9.51$  years old), 174 sessions of N2 sleep (20 males and 24 females; ages:  $28.98 \pm 9.89$  years old), and

195 sessions of N3 sleep (20 males and 21 females; ages:  $26.41 \pm 8.36$  years old) were analyzed in this study (Table S1).

The group-level WM mask is shown in Figure S1. The obtained WM mask showed high symmetry and contained 18,260 voxels in total. WM networks were then obtained based on K-means clustering analysis. Dice coefficients were used to evaluate the stability of the networks. As shown in Figure 1a, the local peak of the Dice coefficients as a function of K was located at  $K = 10$ , which was consistent with the clustering results of some previous studies (Jiang, Luo, et al., 2019; Jiang, Song, et al., 2019; Peer et al., 2017). Therefore, WM networks clustered with  $K = 10$  were adopted for further analysis.

Based on the spatial locations of the networks, these networks were labeled WM1 (superior temporal and motor network), WM2 (frontoparietal network), WM3 (superior frontal and middle temporal gyrus network), WM4 (motor network), WM5 (occipital network), WM6 (brainstem network), WM7 (prefrontal network), WM8 (cerebellar network), WM9 (deep network), and WM10 (parietal network), as shown in Figure 1b. These 10 networks were adopted for the following analyses. In accordance with previous studies, the WM network could be divided into three layers by spatial location, namely, superficial, middle, and deep layers, as shown in Figure 1c. Specific information about these networks is presented in Table 1.

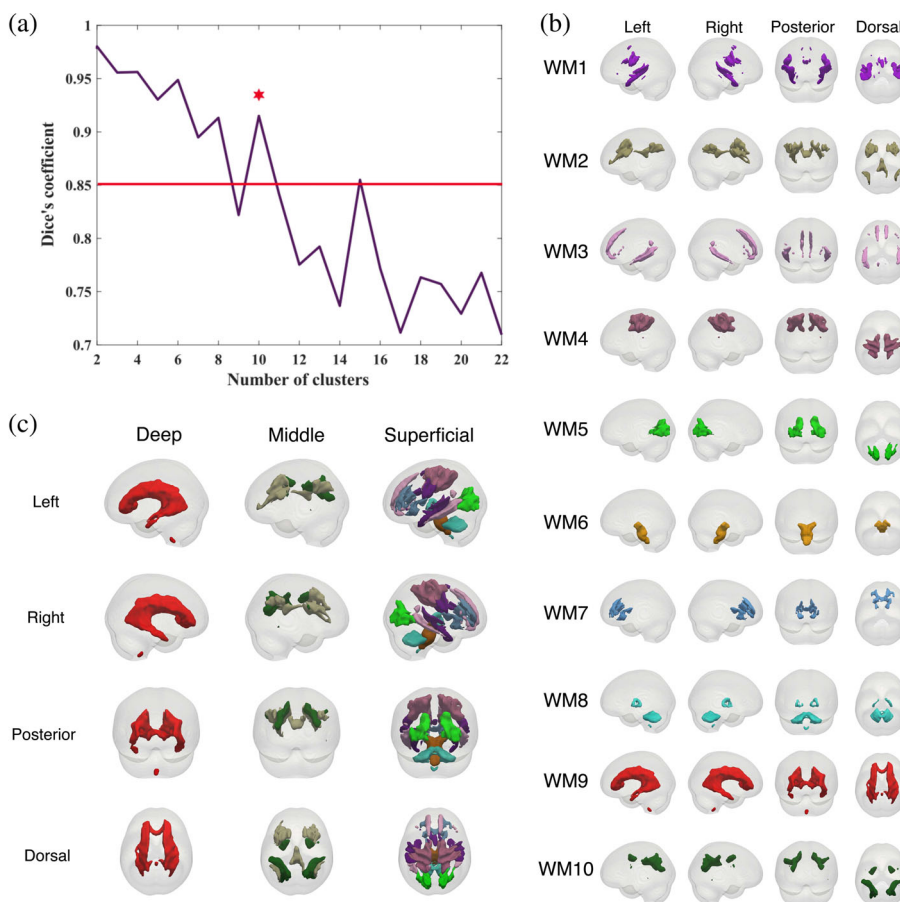


**FIGURE 1** Stability of clustering results of white matter functional networks and spatial locations of white matter functional networks with an optimal number of clusters, that is,  $K = 10$ . (a) Stability of clustering results of white matter functional networks for different numbers of clusters evaluated by Dice coefficients (\* represented the local peak greater than 0.85). (b) Four different views for each of the 10 white matter functional networks. (c) Spatial layout of the 10 white matter functional networks categorized into deep, middle, and superficial layers.

**TABLE 1** Spatial information of white-matter functional networks

Label	White-matter network	Layer	Number of voxels
WM1	Superior temporal and motor network	Superficial	1679
WM2	Fronto-parietal network	Middle	1958
WM3	Superior frontal and middle temporal gyrus network	Superficial	1375
WM4	Motor network	Superficial	2504
WM5	Occipital network	Superficial	1332
WM6	Brainstem network	Superficial	1102
WM7	Prefrontal network	Superficial	1151
WM8	Cerebellar network	Superficial	1350
WM9	Deep network	Deep	4471
WM10	Parietal network	Middle	1338

### 3.2 | Functional connectivity between WM networks during wakefulness and NREM sleep

To explore the functional synchronization between different WM networks, functional connectivity between each pair of the 10 WM networks was calculated, and then the main effect of stage was assessed across the four physiological states, as shown in Figure 2a. After Bonferroni correction ( $p < 10^{-16}$ ), five pairs of WM networks showed a significant main effect of stage (Figure 2b). Functional connectivity between superficial WM networks 1 and 4 and networks 3 and 4, between superficial and middle layer networks 1 and 10 and networks 4 and 10, and between superficial and deep networks 8 and 9 showed significant main effects of physiological state. In general, post hoc analysis showed decreased WM functional connectivity between superficial-superficial and superficial-middle layer WM networks from wakefulness to NREM sleep. Interestingly, functional connectivity between the deep and cerebellar networks was higher during light sleep (N1 and N2) and lower during both wakefulness and deep sleep (Figure 2c). With a less stringent threshold ( $p < .05$ , Bonferroni corrected), a main effect was observed between most pairs of WM networks.

### 3.3 | Characteristics of fluctuation strength in WM networks

To further explore the characteristics of BOLD signals in the WM networks, power spectra were calculated by extracting the average time courses within the network. The power spectra in these WM networks showed similar changes across physiological states (Figure 3). As the frequency increased, the amplitude gradually decreased, which was consistent with the findings in GM (Biswal et al., 1995; Zuo et al., 2010). It is worth noting that two peaks appear in the spectrograms of superficial layer network 6 and deep layer network 9, while only one peak was observed in the spectrograms of other WM networks.

The main effect of stage ( $p < 10^{-16}$ , Bonferroni corrected) showed that for the frequency range of 0.01–0.08 Hz, the average fluctuation amplitudes in superficial layer networks 1, 7, and 8 and deep network 9 were significantly different across states (Figure 4). Post hoc analysis showed that the regional fluctuation amplitude was always higher during light sleep and lower during deep sleep. In addition, the signal amplitudes in superficial layer networks 1 and 8 and deep network 9 were lower during wakefulness than during light sleep, while the amplitudes of superficial layer network 7 and deep network 9 were higher during wakefulness than during deep sleep.

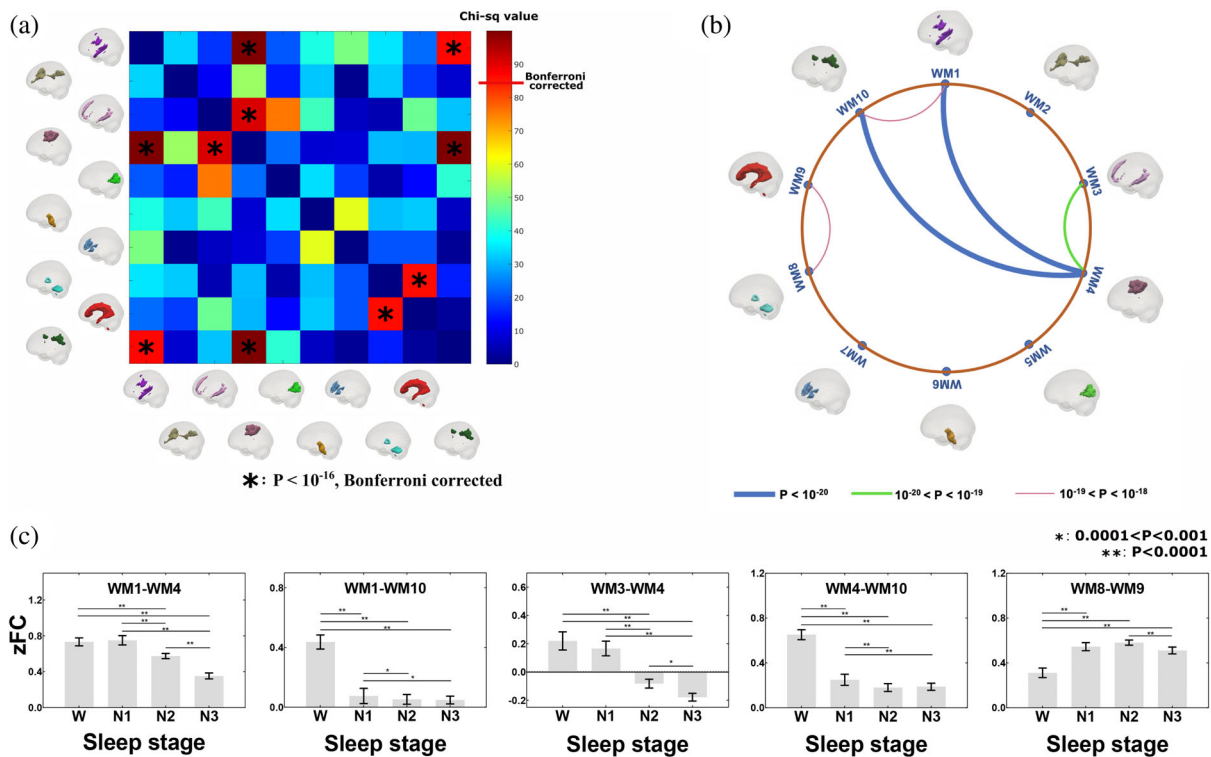


**FIGURE 2** Main effect of sleep stage on functional connectivity between white matter functional networks. (a) Differences in functional connectivity between all the white matter functional networks across stages (the color bar shows the chi-square values. \* represents a significant main effect of stage after Bonferroni correction.) (b) Five pairs of white matter functional networks, which showed a significant main effect of stage. (c) Post hoc results of the five network pairs exhibiting significant main effects are shown in the bottom panel. Functional connectivity is presented as the mean  $\pm$  SEM.

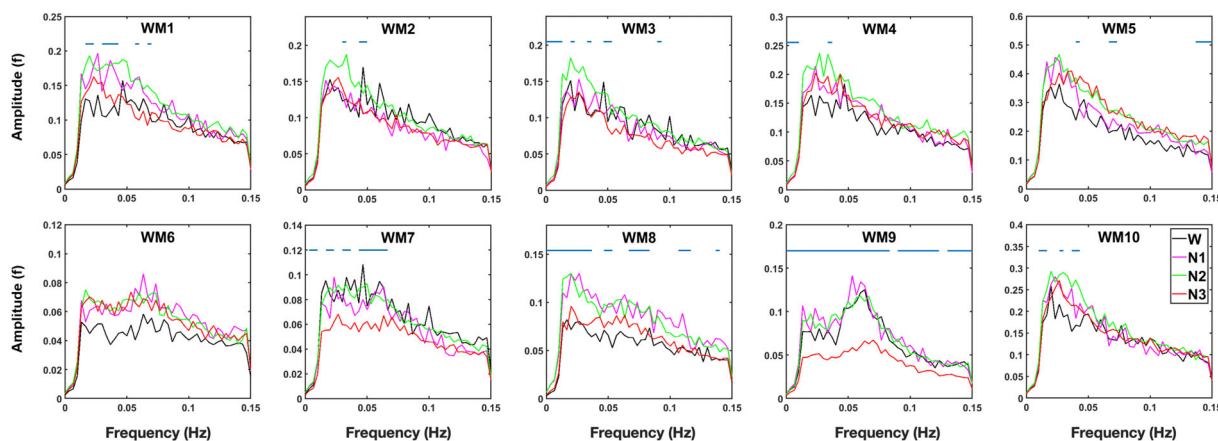


**FIGURE 3** Power spectra of the 10 white matter functional networks. Significant spectral changes ( $p < .05$ , Bonferroni corrected by the number of frequency bins) are indicated by the blue horizontal lines.

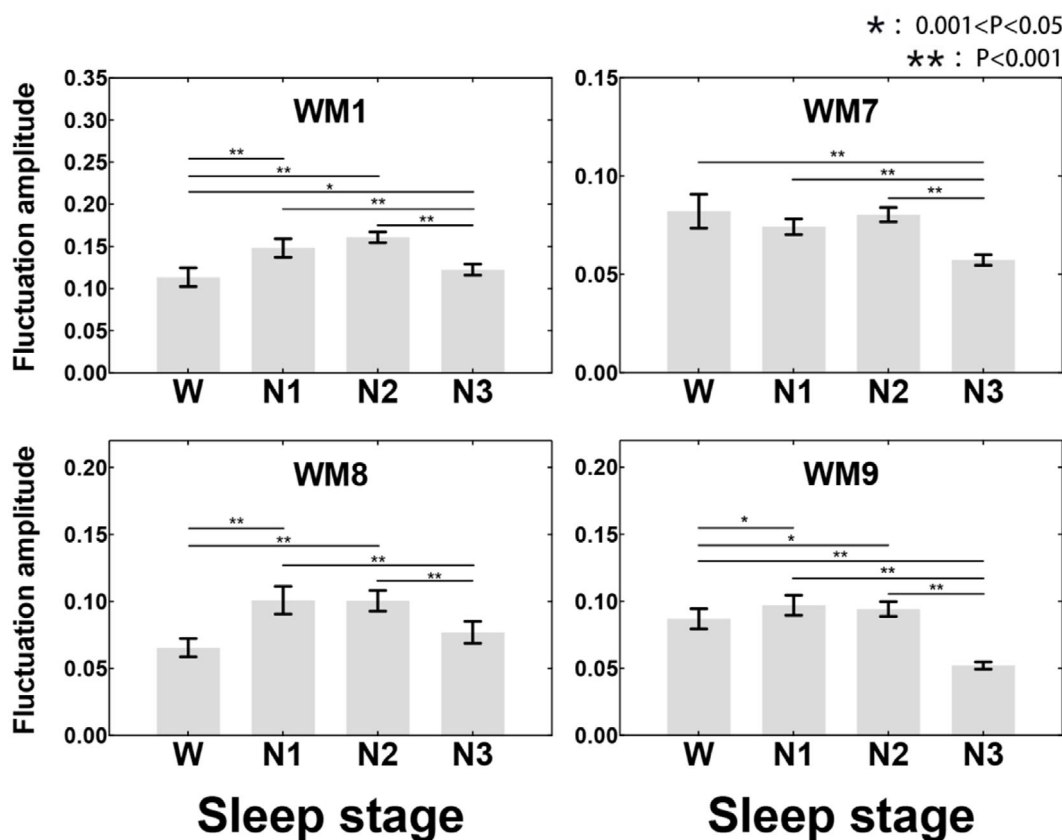


**FIGURE 4** White matter functional networks that showed a significant main effect of stage ( $p < 10^{-16}$ , Bonferroni corrected) and post hoc results on the average fluctuation amplitude within 0.01–0.08 Hz. Data are presented as the mean  $\pm$  SEM.

Further splitting the low-frequency fluctuations into slow-4 (0.027–0.073 Hz) and slow-5 (0.01–0.027 Hz) subbands, we found that for slow-4, the average fluctuation amplitudes in superficial layer networks 1, 7, and 8 and the deep network were significantly different across stages (Figure 5), similar to the findings based on the low-frequency band (Figure 4). Regarding the slow-5 subband, only the average fluctuation amplitude in the deep network was significantly

different across stages (Figure 6), showing similar post hoc findings to those with the low-frequency fluctuations (Figure 3).

Significant interaction effects between physiological states and different subbands regarding the fluctuation amplitudes in the occipital network (WM5) and the deep network ( $p < .001$ , Bonferroni corrected) were observed (Figure 7). Taking the occipital network as an example, post hoc analysis showed higher fluctuation amplitude in

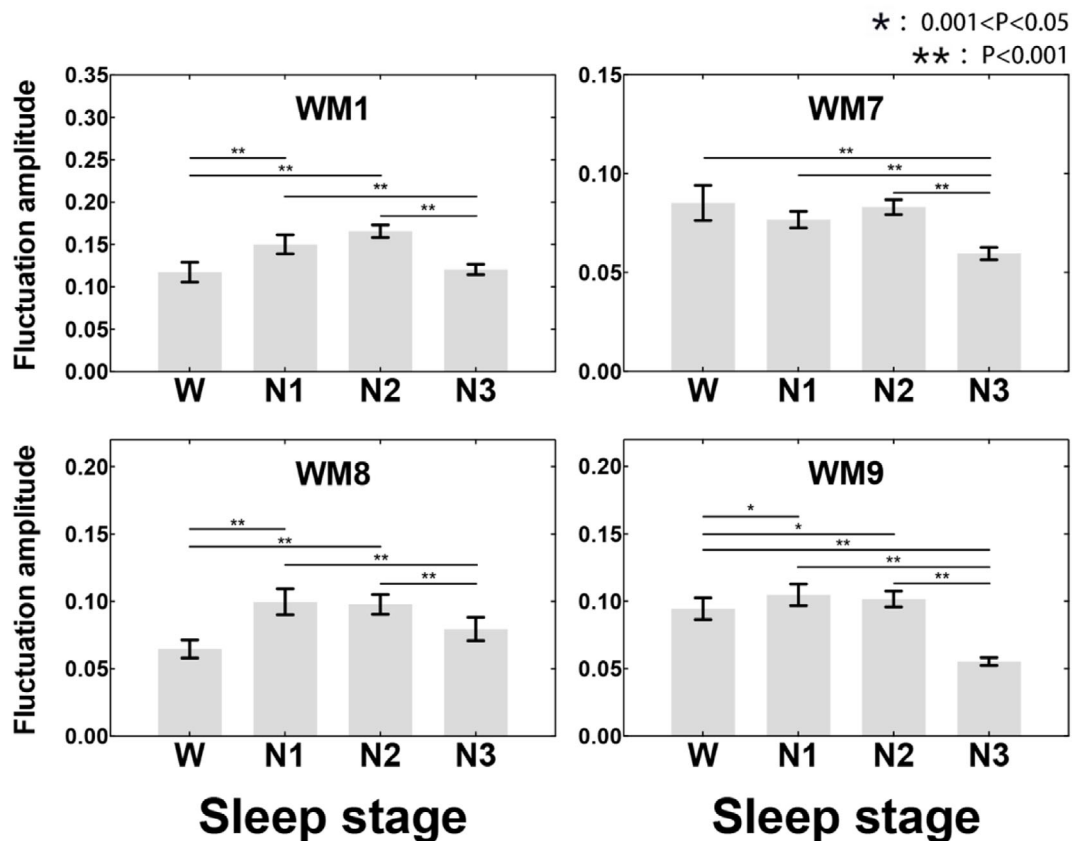


**FIGURE 5** White matter functional networks that showed a significant main effect of stage ( $p < .001$ , Bonferroni corrected) and post hoc results on the average fluctuation amplitude within the slow-4 subband (0.027–0.073 Hz). Data are presented as the mean  $\pm$  SEM.

slow-5 than slow-4 during N1 and N2 sleep but lower fluctuation amplitude in slow-5 than slow-4 during N3 sleep. Regarding the deep network, although slow-4 always showed a higher amplitude across the four stages, the extent of the increase was smaller during N3.

Meanwhile, significant main effects of subbands were observed in the superficial white networks located in the middle temporal, frontal and brainstem networks, the middle layer parietal network and the deep WM network (Table 2). In addition, significant stage effects on fluctuation amplitude were found in all 10 WM networks.

### 3.4 | Correlations between slow-wave activity and characteristics of WM networks

For the five pairs of WM networks that showed significant stage effects (Figure 2), exploratory correlation analysis between EEG SWA during stage N3 and WM network connectivity was performed. Connectivity between all five pairs of WM networks negatively correlated with SWA power (Figure 8).

Regarding the fluctuation amplitude of BOLD signals within WM networks 1, 7, 8, and 9 that showed a significant stage effect (Figure 4), a similar correlation analysis with SWA during N3 was conducted. SWA was positively correlated with fluctuation amplitude in

superficial layer WM networks 1, 7 and 8, while there was no significant correlation with deep WM network 9 (Figure 9).

## 4 | DISCUSSION

It is generally believed that BOLD signals in GM reflect neuronal activity. Recent studies have shown reliable BOLD signals in WM, which seem to reflect intrinsic neuronal activity (Gawryluk et al., 2014; Gore et al., 2019). Task activation in the corpus callosum while performing specific tasks (Gawryluk et al., 2011; Mazerolle et al., 2008; Mazerolle et al., 2010) has been observed. Furthermore, fMRI signals in WM could be clustered into multiple functional networks (Jiang, Song, et al., 2019; Peer et al., 2017), which closely correspond to WM tracts identified by diffusion tensor imaging. In this study, 10 stable WM functional networks (WM1–WM10, including superficial, middle, and deep networks) were obtained by a clustering analysis based on the fMRI data during wakefulness and NREM sleep (N1, N2, and N3 sleep). Functional connectivity between the WM networks was calculated, and the comparison showed that from wakefulness to sleep, WM functional connectivity between superficial and middle layer WM networks decreased. Interestingly, the functional connectivity between the deep and cerebellar networks was lower during both wakefulness and deep sleep but higher during light sleep. Moreover,



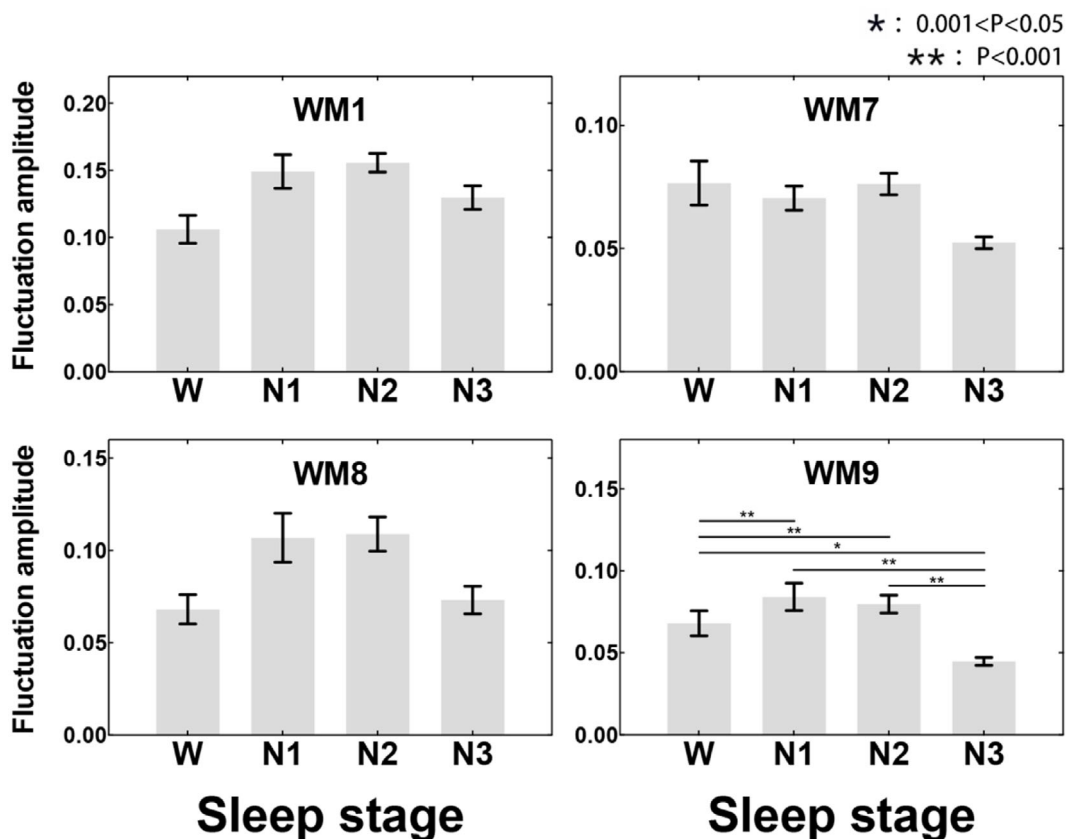
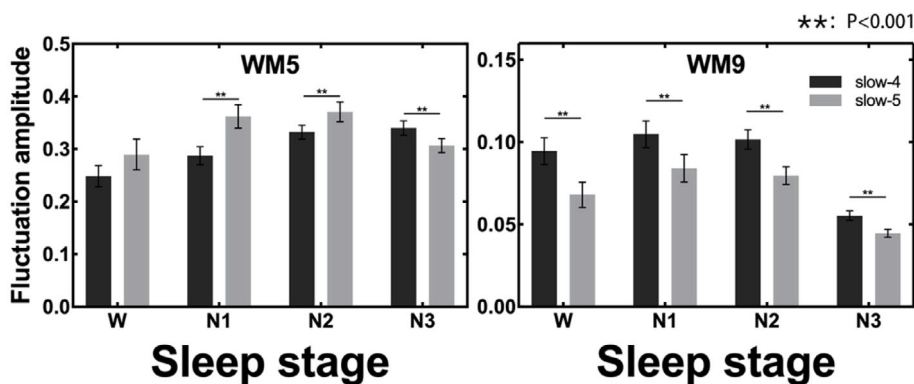


**FIGURE 6** White matter functional networks that showed a significant main effect of stage ( $p < .001$ , Bonferroni corrected) and post hoc results on the average fluctuation amplitude within the slow-5 subband (0.01–0.027 Hz). Data are presented as the mean ± SEM was presented.

**FIGURE 7** White matter functional networks that showed a significant interaction effect between stage and subband on the average fluctuation amplitude ( $p < .001$ , Bonferroni corrected). Data are presented as the mean ± SEM.



the regional amplitude of WM signal fluctuations across multiple low-frequency bands was evaluated and showed that the regional fluctuation amplitude was always higher during light sleep and lower during deep sleep. Additionally, the signal amplitudes in the superior temporal, cerebellar and deep WM networks were higher during light sleep than during wakefulness. Furthermore, we found that the signal fluctuated more strongly in the slow-4 band than that of slow-5 across the WM during wakefulness and NREM sleep. Finally, based on the above results, to investigate whether the difference in functional connectivity or frequency characteristics had some electrophysiological meaning, the correlations between SWA and the above significant

differences were analyzed. The results showed that SWA during deep sleep was negatively correlated with functional connectivity between WM networks but positively correlated with the frequency amplitude in WM, which provides direct physiological evidence that neural activities in WM are modulated by the sleep-wake cycle.

Functional connectivity has been widely used in neuroscience and clinical practice and reflects the temporal synchronization in spontaneous fluctuations between brain regions (Biswal et al., 1995) or networks (Smith et al., 2015). Previous WM connectivity studies have shown that fluctuations in WM BOLD signals are related to neural activities (Gore et al., 2019). In the present study, functional

Label	p value		
	Interaction effect	Main effect of sub-band	Main effect of stage
WM1	>.05	>.05	$5.69 \times 10^{-21}$
WM2	>.05	$6.67 \times 10^{-3}$	$2.14 \times 10^{-14}$
WM3	>.05	$1.72 \times 10^{-4}$	$1.80 \times 10^{-19}$
WM4	>.05	>.05	$8.94 \times 10^{-17}$
WM5	$1.29 \times 10^{-11}$	$4.18 \times 10^{-3}$	$1.05 \times 10^{-11}$
WM6	>.05	$3.71 \times 10^{-7}$	$1.17 \times 10^{-11}$
WM7	>.05	$1.01 \times 10^{-6}$	$1.93 \times 10^{-21}$
WM8	$2.38 \times 10^{-3}$	>.05	$1.93 \times 10^{-21}$
WM9	$5.05 \times 10^{-7}$	$1.93 \times 10^{-21}$	$1.93 \times 10^{-21}$
WM10	>.05	$1.36 \times 10^{-6}$	$3.65 \times 10^{-17}$

**TABLE 2** Interaction and main effects of sub-band on fluctuation amplitude in all WM functional networks

Note: p values were Bonferroni corrected, and those marked in bold font could survive correction.

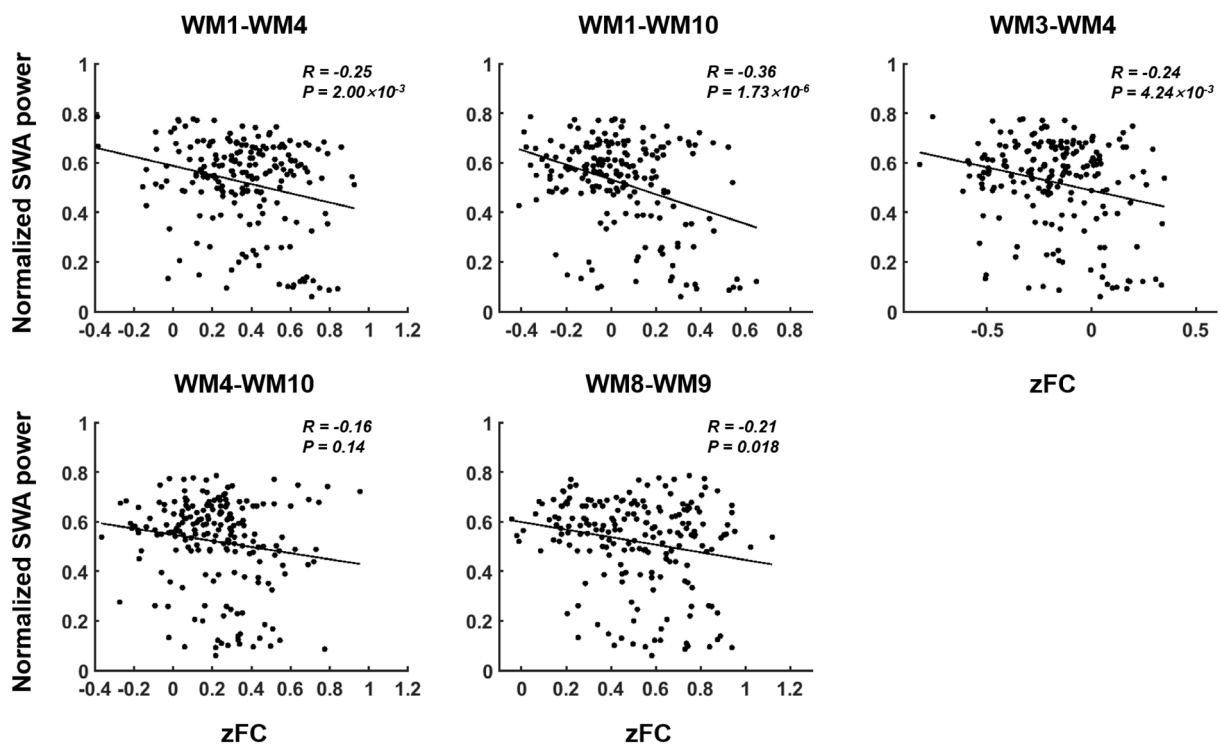


**FIGURE 8** Significant correlations (corrected by the number of white matter networks adopted in the correlation analyses) of functional connectivity between white matter functional networks and slow-wave activity (SWA)

connectivity between WM networks was calculated during varying physiological stages, including wakefulness and NREM sleep. Analyses of the main effect of stage were performed to detect the differences among the four sleep states. Functional connectivity between superficial layer WM networks, between superficial and middle layer WM networks, and between superficial and deep layer WM networks showed significant main effects of stage, indicating that each physiological stage was associated with a specific level of functional connectivity. Further post hoc analysis found that functional connectivity between four pairs of superficial–superficial and superficial–middle layer WM networks decreased from wakefulness to N3 sleep. Our

findings in WM networks are similar to those obtained in GM networks. Awareness and responsiveness to environmental stimuli show physiologically distinct changes during sleep compared with wakefulness (Larson-Prior et al., 2009). Fading of consciousness during NREM sleep has been demonstrated to be associated with a breakdown in cortical effective connectivity (Massimini et al., 2005). Temporal integration, measured as long-term memory in the history of neural activity, gradually decreases from wakefulness to deep sleep (Tagliazucchi et al., 2013).

It should be noted that functional connectivity between the cerebellar network and deep layer WM network under NREM sleep was

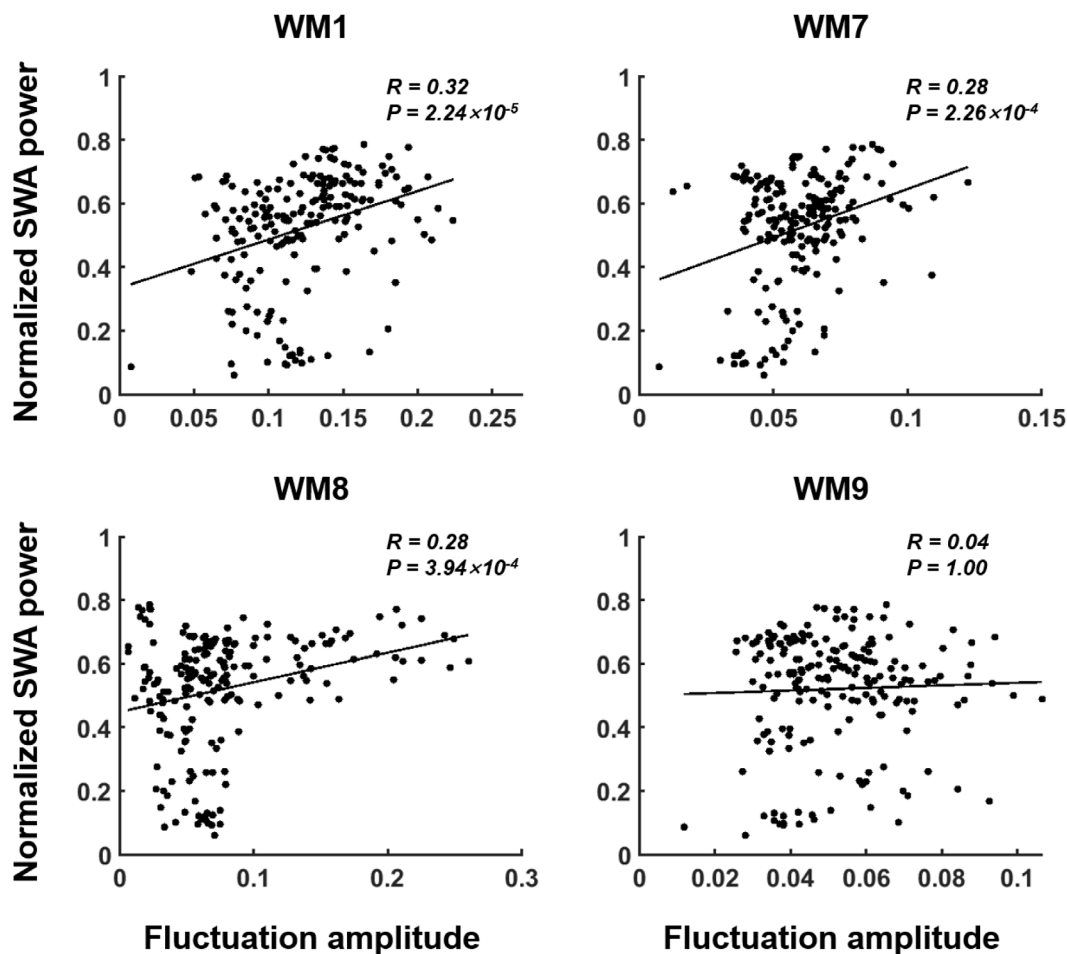


**FIGURE 9** Significant correlation (corrected by the number of white matter networks adopted in the correlation analyses) between the average fluctuation amplitude in white matter functional networks and slow-wave activity (SWA)

higher than that under wakefulness. The increased internetwork connectivity between parietal and cerebellar WM networks during deep sleep might support memory consolidation (Vahdat et al., 2017). Nonetheless, future studies linking WM internetwork connectivity with cognition and behavior are warranted.

The regional characteristics of WM networks were further investigated using the fluctuation amplitude of each WM network. A gradual decrease in amplitude with increased frequency during wakefulness was observed, which was identical to a previous study (Peer et al., 2017). Importantly, the average fluctuation amplitudes in the superior temporal and motor networks, prefrontal network, cerebellar network and deep network showed significant differences across the four physiological stages of sleep, indicating that different physiological stages were associated with divergent strengths of low-frequency fluctuations. Further post hoc analysis showed that the mean fluctuation amplitude in the superior temporal and motor network, cerebellar network and deep network increased from wakefulness to light sleep (N1 and N2 sleep stages) and then decreased when entering deep sleep. N1 sleep is generally short and unstable, while N2 sleep is characterized by K-complex and spindle waves, which might cause a larger amplitude of signal fluctuations. Thus, the

average fluctuation amplitudes of N1 and N2 sleep were larger than those of wakefulness and N3 sleep. It is worth noting that spindle activity is related to sleep-dependent memory enhancements (Crunelli et al., 2018), and spindles during N2 sleep seem to support memory consolidation (Gais et al., 2002). Thus, the difference in mean fluctuation amplitude is probably associated with memory consolidation during sleep, which should be investigated in more detail in future studies. Moreover, Zhou et al. investigated dynamic functional connectivity states during wakefulness and NREM sleep and found that the number of state transitions showed a trend of an increase from wakefulness to N2 sleep and decrease (Zhou et al., 2019) in N3 sleep. In addition, Kung and colleagues showed the highest instability of information transfer within and between functional networks during N2 sleep (Kung et al., 2019). The average fluctuation amplitude of the deep layer network increased from wakefulness to N1 sleep and gradually decreased from N1 sleep to N3 sleep, which was similar to the trend in GM signal variance across sleep stages (Tagliazucchi et al., 2013).

Consistent with previous studies (Jiang, Luo, et al., 2019; Peer et al., 2017), the average fluctuation amplitudes in the deep layer network had two peaks in the low-frequency band during wakefulness.

We extended this finding such that the pattern of the two-peak power spectrum was maintained during both light and deep sleep. Furthermore, the low-frequency band was divided into slow-4 and slow-5 subbands, and the fluctuation amplitudes of WM networks across sleep stages were compared. The results showed that the average fluctuation amplitude in slow-4, much more than that in slow-5, contributed to the main findings of fluctuation amplitude in the low-frequency band. The two-peak power spectrum and the characteristics of the slow-4 phenomenon need to be investigated in future studies.

SWA is a typical neural pattern of behavior observed during sleep, the power of which is higher during NREM sleep than during wakefulness, and it is a common electrophysiological signature of sleep pressure (Léger et al., 2018). There was a significant negative correlation between SWA and functional connectivity between superficial-superficial and superficial-middle layer WM networks under N3 sleep. Correspondence between inter-WM network connectivity and SWA provided direct evidence that functional connectivity between WM networks has electrophysiological significance. In contrast, the fluctuation amplitude of three superficial WM networks was positively correlated with SWA during deep sleep. Thus, decreased between-network integration with increased local fluctuation amplitude in the WM networks are associated with sleep pressure and slow-wave generation and propagation.

The results demonstrated in the present study may help improve our understanding of the neural mechanisms for sleep. In particular, the comparisons of regional WM fMRI measurements among different sleep stages and analyses of their relations with EEG signals may yield novel insight into neural the substrates of natural sleep and wakefulness, which could foster major breakthrough in this fundamental neuroscience research. And from a broader perspective, this study expanded the horizon of WM fMRI studies, which may attract an increasing number of scientists to pay close attention to this emerging area.

There were some limitations in this study. First, the number of imaging sessions varies with the sleep stages, among which N1 has fewer sessions than N2 and N3. This is hardly avoidable, however, given that typically the duration of N1 stage (5%–10%) is much shorter than those of N2 (~50%) and N3 (~20%) stages during natural sleeping and we wish to maximize the use of imaging data available. Second, the WM clustering analysis was conducted within the group-level WM mask and performed based on fMRI data from all four physiological stages. It will be useful in future studies to derive precise individualized and stage-specific parcellations in WM functional organization, similar to the construction of cortical parcels (Gordon et al., 2017; Han et al., 2020). To test whether the findings in the main text will be affected by the generation of WM masks, we adopted an independent set of masks for WM networks from Peer and colleagues (Peer et al., 2017). We observed similar results (Table S2 and Figures S1–S4), thus providing validation that our findings are robust and stable. In the end, more analytic methods, such as dynamic functional connectivity and regional homogeneity, should be used to investigate the comprehensive characteristics of WM functional activity.

## ACKNOWLEDGMENTS

This work was supported by the National Key Research and Development Program of China (2018YFC2000603); the National Natural Science Foundation of China (81871427 and 81671765); Beijing United Imaging Research Institute of Intelligent Imaging Foundation (CRIBJZD202101); the Beijing Municipal Science & Technology Commission (Z181100001518005); Sichuan Science and Technology Program (2021JDRC0038). The authors thank the National Center for Protein Sciences at Peking University in Beijing, China, for assistance with MRI data acquisition and data analyses.

## CONFLICT OF INTEREST

The authors declare no conflict of interest.

## DATA AVAILABILITY STATEMENT

The data that support the findings of this study are available from the corresponding author upon reasonable request. The data are not publicly available due to privacy or ethical restrictions.

## ORCID

Binghu Jiang  <https://orcid.org/0000-0003-2707-570X>

Qihong Zou  <https://orcid.org/0000-0001-8732-6633>

## REFERENCES

- Allen, P. J., Josephs, O., & Turner, R. (2000). A method for removing imaging artifact from continuous EEG recorded during functional MRI. *NeuroImage*, *12*, 230–239.
- Allen, P. J., Polizzi, G., Krakow, K., Fish, D. R., & Lemieux, L. (1998). Identification of EEG events in the MR scanner: The problem of pulse artifact and a method for its subtraction. *NeuroImage*, *8*, 229–239.
- Ashburner, J. (2007). A fast diffeomorphic image registration algorithm. *NeuroImage*, *38*, 95–113.
- Biswal, B., Zerrin Yetkin, F., Haughton, V. M., & Hyde, J. S. (1995). Functional connectivity in the motor cortex of resting human brain using echo-planar MRI. *Magnetic Resonance in Medicine*, *34*, 537–541.
- Blumensath, T., Jbabdi, S., Glasser, M. F., Van Essen, D. C., Ugurbil, K., Behrens, T. E. J., & Smith, S. M. (2013). Spatially constrained hierarchical parcellation of the brain with resting-state fMRI. *NeuroImage*, *76*, 313–324.
- Cha, K., Zatorre, R. J., & Schönwiesner, M. (2016). Frequency selectivity of voxel-by-voxel functional connectivity in human auditory cortex. *Cerebral Cortex*, *26*, 211–224.
- Chaarani, B., Hahn, S., Allgaier, N., Adise, S., Owens, M. M., Juliano, A. C., Yuan, D. K., Loso, H., Ivanciu, A., Albaugh, M. D., Dumas, J., Mackey, S., Laurent, J., Ivanova, M., Hagler, D. J., Cornejo, M. D., Hatton, S., Agrawal, A., Aguinaldo, L., ... the, A.C. (2021). Baseline brain function in the preadolescents of the ABCD study. *Nature Neuroscience*, *24*, 1176–1186.
- Chen, G., Saad, Z. S., Britton, J. C., Pine, D. S., & Cox, R. W. (2013). Linear mixed-effects modeling approach to fMRI group analysis. *NeuroImage*, *73*, 176–190.
- Chen, Y., Dang, M., & Zhang, Z. (2021). Brain mechanisms underlying neuropsychiatric symptoms in Alzheimer's disease: A systematic review of symptom-general and -specific lesion patterns. *Molecular Neurodegeneration*, *16*, 38.
- Cox, R. W. (1996). AFNI: Software for analysis and visualization of functional magnetic resonance neuroimages. *Computers and Biomedical Research*, *29*, 162–173.

- Craddock, R. C., James, G. A., Holtzheimer, P. E., Hu, X. P., & Mayberg, H. S. (2012). A whole brain fMRI atlas generated via spatially constrained spectral clustering. *Human Brain Mapping*, 33, 1914–1928.
- Crunelli, V., Lőrincz, M. L., Connelly, W. M., David, F., Hughes, S. W., Lambert, R. C., Leresche, N., & Errington, A. C. (2018). Dual function of thalamic low-vigilance state oscillations: Rhythm-regulation and plasticity. *Nature Reviews. Neuroscience*, 19, 107–118.
- Ding, J.-R., Ding, X., Hua, B., Xiong, X., Wen, Y., Ding, Z., Wang, Q., & Thompson, P. (2018). Altered connectivity patterns among resting state networks in patients with ischemic white matter lesions. *Brain Imaging and Behavior*, 12, 1239–1250.
- Ding, Z., Huang, Y., Bailey, S. K., Gao, Y., Cutting, L. E., Rogers, B. P., Newton, A. T., & Gore, J. C. (2018). Detection of synchronous brain activity in white matter tracts at rest and under functional loading. *Proceedings of the National Academy of Sciences of the United States of America*, 115, 595–600.
- Ding, Z., Newton, A. T., Xu, R., Anderson, A. W., Morgan, V. L., & Gore, J. C. (2013). Spatio-temporal correlation tensors reveal functional structure in human brain. *PLoS One*, 8, e82107.
- Duan, X., Chen, H., He, C., Long, Z., Guo, X., Zhou, Y., Uddin, L. Q., & Chen, H. (2017). Resting-state functional under-connectivity within and between large-scale cortical networks across three low-frequency bands in adolescents with autism. *Progress in Neuro-Psychopharmacology and Biological Psychiatry*, 79, 434–441.
- Fox, M. D., & Raichle, M. E. (2007). Spontaneous fluctuations in brain activity observed with functional magnetic resonance imaging. *Nature Reviews Neuroscience*, 8, 700–711.
- Friston, K. J., Williams, S., Howard, R., Frackowiak, R. S. J., & Turner, R. (1996). Movement-related effects in fMRI time-series. *Magnetic Resonance in Medicine*, 35, 346–355.
- Gais, S., Mölle, M., Helms, K., & Born, J. (2002). Learning-dependent increases in sleep spindle density. *The Journal of Neuroscience: The Official Journal of the Society for Neuroscience*, 22, 6830–6834.
- Gawryluk, J. R., Brewer, K. D., Beyea, S. D., & D'Arcy, R. C. N. (2009). Optimizing the detection of white matter fMRI using asymmetric spin echo spiral. *NeuroImage*, 45, 83–88.
- Gawryluk, J. R., D'Arcy, R. C. N., Mazerolle, E. L., Brewer, K. D., & Beyea, S. D. (2011). Functional mapping in the corpus callosum: A 4T fMRI study of white matter. *NeuroImage*, 54, 10–15.
- Gawryluk, J. R., Mazerolle, E. L., & D'Arcy, R. C. N. (2014). Does functional MRI detect activation in white matter? A review of emerging evidence, issues, and future directions. *Frontiers in Neuroscience*, 8, 239.
- Gordon, E. M., Laumann, T. O., Gilmore, A. W., Newbold, D. J., Greene, D. J., Berg, J. J., Ortega, M., Hoyt-Drazen, C., Grattton, C., Sun, H., Hampton, J. M., Coalson, R. S., Nguyen, A. L., McDermott, K. B., Shimony, J. S., Snyder, A. Z., Schlaggar, B. L., Petersen, S. E., Nelson, S. M., & Dosenbach, N. U. F. (2017). Precision functional mapping of individual human brains. *Neuron*, 95, 791–807. e797.
- Gore, J. C., Li, M., Gao, Y., Wu, T.-L., Schilling, K. G., Huang, Y., Mishra, A., Newton, A. T., Rogers, B. P., Chen, L. M., Anderson, A. W., & Ding, Z. (2019). Functional MRI and resting state connectivity in white matter - a mini-review. *Magnetic Resonance Imaging*, 63, 1–11.
- Grauskas, L. A., Frizzell, T., Song, X., & D'Arcy, R. C. N. (2019). White matter fMRI activation cannot be treated as a nuisance regressor: Overcoming a historical blind spot. *Frontiers in neuroscience*, 13, 1024.
- Han, M., Yang, G., Li, H., Zhou, S., Xu, B., Jiang, J., Men, W., Ge, J., Gong, G., Liu, H., & Gao, J. H. (2020). Individualized cortical parcellation based on diffusion MRI tractography. *Cerebral Cortex*, 30, 3198–3208.
- Helenius, J., Perkiö, J., Soine, L., Østergaard, L., Carano, R. A. D., Salonen, O., Savolainen, S., Kaste, M., Aronen, H. J., & Tatlisumak, T. (2003). Cerebral hemodynamics in a healthy population measured by dynamic susceptibility contrast MR imaging. *Acta Radiologica*, 44, 538–546.
- Hill, P. F., King, D. R., Lega, B. C., & Rugg, M. D. (2020). Comparison of fMRI correlates of successful episodic memory encoding in temporal lobe epilepsy patients and healthy controls. *NeuroImage*, 207, 116397.
- Iber, C., Ancoli-Israel, S., Chesson, A. L., & Quan, S. (2007). *The AASM manual for the scoring of sleep and associated events: Rules, terminology and technical specifications*. American Academy of Sleep Medicine.
- Ji, G. U., Ren, C., Li, Y., Sun, J., Liu, T., Gao, Y., Xue, D., Shen, L., Cheng, W., & Zhu, C. J. H. B. M. (2019). Regional and network properties of white matter function in Parkinson's disease. *Human Brain Mapping*, 40, 1253–1263.
- Jiang, Y., Luo, C., Li, X., Li, Y., Yang, H., Li, J., Chang, X., Li, H., Yang, H., Wang, J., Duan, M., & Yao, D. (2019). White-matter functional networks changes in patients with schizophrenia. *NeuroImage*, 190, 172–181.
- Jiang, Y., Song, L., Li, X., Zhang, Y., Chen, Y., Jiang, S., Hou, C., Yao, D., Wang, X., & Luo, C. (2019). Dysfunctional white-matter networks in medicated and unmedicated benign epilepsy with centrotemporal spikes. *Human Brain Mapping*, 40, 3113–3124.
- Kung, Y.-C., Li, C.-W., Chen, S., Chen, S. C.-J., Lo, C.-Y. Z., Lane, T. J., Biswal, B., Wu, C. W., & Lin, C.-P. (2019). Instability of brain connectivity during nonrapid eye movement sleep reflects altered properties of information integration. *Human Brain Mapping*, 40, 3192–3202.
- Lange, T., Roth, V., Braun, M., & Buhmann, J. (2004). Stability-based validation of clustering solutions. *Neural Computation*, 16, 1299–1323.
- Larson-Prior, L. J., Zempel, J. M., Nolan, T. S., Prior, F. W., Snyder, A. Z., & Raichle, M. E. (2009). Cortical network functional connectivity in the descent to sleep. *Proceedings of the National Academy of Sciences of the United States of America*, 106, 4489–4494.
- Léger, D., Debellemanni, E., Rabat, A., Bayon, V., Benchenane, K., & Chennaoui, M. (2018). Slow-wave sleep: From the cell to the clinic. *Sleep Medicine Reviews*, 41, 113–132.
- Li, J., Biswal, B. B., Wang, P., Duan, X., Cui, Q., Chen, H., & Liao, W. (2019). Exploring the functional connectome in white matter. *Human Brain Mapping*, 40, 4331–4344.
- Li, M., Gao, Y., Ding, Z., & Gore, J. C. (2021). Power spectra reveal distinct BOLD resting-state time courses in white matter. *Proceedings of the National Academy of Sciences*, 118, e2103104118.
- Li, Q., Tavakol, S., Royer, J., Larivière, S., Vos De Wael, R., Park, B.-Y., Paquola, C., Zeng, D., Caldaïrou, B., Bassett, D. S., Bernasconi, A., Bernasconi, N., Frauscher, B., Smallwood, J., Caciagli, L., Li, S., & Bernhardt, B. C. (2021). Atypical neural topographies underpin dysfunctional pattern separation in temporal lobe epilepsy. *Brain: A Journal of Neurology*, 144, 2486–2498.
- Ly, J. Q. M., Gaggioli, G., Chellappa, S. L., Papachilleos, S., Brzozowski, A., Borsu, C., Rosanova, M., Sarasso, S., Middleton, B., Luxen, A., Archer, S. N., Phillips, C., Dijk, D.-J., Maquet, P., Massimini, M., & Vandewalle, G. (2016). Circadian regulation of human cortical excitability. *Nature Communications*, 7, 11828.
- Massimini, M., Ferrarelli, F., Huber, R., Esser, S. K., Singh, H., & Tononi, G. (2005). Breakdown of cortical effective connectivity during sleep. *Science (New York, N.Y.)*, 309, 2228–2232.
- Mazerolle, E. L., Beyea, S. D., Gawryluk, J. R., Brewer, K. D., Bowen, C. V., & D'Arcy, R. C. N. (2010). Confirming white matter fMRI activation in the corpus callosum: Co-localization with DTI tractography. *NeuroImage*, 50, 616–621.
- Mazerolle, E. L., D'Arcy, R. C. N., & Beyea, S. D. (2008). Detecting functional magnetic resonance imaging activation in white matter: Inter-hemispheric transfer across the corpus callosum. *BMC Neuroscience*, 9, 84.
- Moreno-Dominguez, D., Anwender, A., & Knösche, T. R. (2014). A hierarchical method for whole-brain connectivity-based parcellation. *Human Brain Mapping*, 35, 5000–5025.
- Omura, K., Tsukamoto, T., Kotani, Y., Ohgami, Y., Minami, M., & Inoue, Y. (2004). Different mechanisms involved in interhemispheric transfer of visuomotor information. *Neuroreport*, 15, 2707–2711.

- Palva, J. M., & Palva, S. (2012). Infra-slow fluctuations in electrophysiological recordings, blood-oxygenation-level-dependent signals, and psychophysical time series. *NeuroImage*, *62*, 2201–2211.
- Peer, M., Nitzan, M., Bick, A. S., Levin, N., & Arzy, S. (2017). Evidence for functional networks within the human brain's white matter. *The Journal of Neuroscience: The Official Journal of the Society for Neuroscience*, *37*, 6394–6407.
- Peer, M., Nitzan, M., Goldberg, I., Katz, J., Gomori, J. M., Ben-Hur, T., & Arzy, S. (2014). Reversible functional connectivity disturbances during transient global amnesia. *Annals of Neurology*, *75*, 634–643.
- Preibisch, C., & Haase, A. (2001). Perfusion imaging using spin-labeling methods: Contrast-to-noise comparison in functional MRI applications. *Magnetic Resonance in Medicine*, *46*, 172–182.
- Rostrup, E., Law, I., Blinkenberg, M., Larsson, H. B. W., Born, A. P., Holm, S., & Paulson, O. B. (2000). Regional differences in the CBF and BOLD responses to hypercapnia: A combined PET and fMRI study. *NeuroImage*, *11*, 87–97.
- Smith, S. M., Nichols, T. E., Vidaurre, D., Winkler, A. M., Behrens, T. E. J., Glasser, M. F., Ugurbil, K., Barch, D. M., Van Essen, D. C., & Miller, K. L. (2015). A positive-negative mode of population covariation links brain connectivity, demographics and behavior. *Nature Neuroscience*, *18*, 1565–1567.
- Tagliazucchi, E., von Wegner, F., Morzelewski, A., Brodbeck, V., Jahnke, K., & Laufs, H. (2013). Breakdown of long-range temporal dependence in default mode and attention networks during deep sleep. *Proceedings of the National Academy of Sciences*, *110*, 15419–15424.
- Tettamanti, M., Paulesu, E., Scifo, P., Maravita, A., Fazio, F., Perani, D., & Marzi, C. A. (2002). Interhemispheric transmission of visuomotor information in humans: fMRI evidence. *Journal of Neurophysiology*, *88*, 1051–1058.
- Vahdat, S., Fogel, S., Benali, H., & Doyon, J. (2017). Network-wide reorganization of procedural memory during NREM sleep revealed by fMRI. *eLife*, *6*, e24987.
- Van Dijk, K. R. A., Hedden, T., Venkataraman, A., Evans, K. C., Lazar, S. W., & Buckner, R. L. (2009). Intrinsic functional connectivity as a tool for human connectomics: Theory, properties, and optimization. *Journal of Neurophysiology*, *103*, 297–321.
- Weber, B., Treyer, V., Oberholzer, N., Jaermann, T., Boesiger, P., Brugger, P., Regard, M., Buck, A., Savazzi, S., & Marzi, C. A. (2005). Attention and interhemispheric transfer: A behavioral and fMRI study. *Journal of Cognitive Neuroscience*, *17*, 113–123.
- Wolters, A. F., van de Weijer, S. C. F., Leentjens, A. F. G., Duits, A. A., Jacobs, H. I. L., & Kuijf, M. L. (2019). Resting-state fMRI in Parkinson's disease patients with cognitive impairment: A meta-analysis. *Parkinsonism & Related Disorders*, *62*, 16–27.
- Yan, C.-G., & Zang, Y.-F. (2010). DPARSF: A MatLab toolbox for "pipeline" data analysis of resting-state fMRI. *Frontiers in Systems Neuroscience*, *4*, 13.
- Yeo, B. T. T., Krienen, F. M., Sepulcre, J., Sabuncu, M. R., Lashkari, D., Hollinshead, M., Roffman, J. L., Smoller, J. W., Zöllei, L., Polimeni, J. R., Fischl, B., Liu, H., & Buckner, R. L. (2011). The organization of the human cerebral cortex estimated by intrinsic functional connectivity. *Journal of Neurophysiology*, *106*, 1125–1165.
- Zang, Y.-F., He, Y., Zhu, C.-Z., Cao, Q.-J., Sui, M.-Q., Liang, M., Tian, L.-X., Jiang, T.-Z., & Wang, Y.-F. (2006). Altered baseline brain activity in children with ADHD revealed by resting-state functional MRI. *Brain & Development*, *29*, 83–91.
- Zhou, S., Zou, G., Xu, J., Su, Z., Zhu, H., Zou, Q., & Gao, J.-H. (2019). Dynamic functional connectivity states characterize NREM sleep and wakefulness. *Human Brain Mapping*, *40*, 5256–5268.
- Zou, G., Li, Y., Liu, J., Zhou, S., Xu, J., Qin, L., Shao, Y., Yao, P., Sun, H., Zou, Q., & Gao, J.-H. (2021). Altered thalamic connectivity in insomnia disorder during wakefulness and sleep. *Human Brain Mapping*, *42*, 259–270.
- Zuo, X.-N., Di Martino, A., Kelly, C., Shehzad, Z. E., Gee, D. G., Klein, D. F., Castellanos, F. X., Biswal, B. B., & Milham, M. P. (2010). The oscillating brain: Complex and reliable. *NeuroImage*, *49*, 1432–1445.

#### SUPPORTING INFORMATION

Additional supporting information may be found in the online version of the article at the publisher's website.

**How to cite this article:** Yang, Y., Wang, S., Liu, J., Zou, G., Jiang, J., Jiang, B., Cao, W., & Zou, Q. (2022). Changes in white matter functional networks during wakefulness and sleep. *Human Brain Mapping*, *43*(14), 4383–4396. <https://doi.org/10.1002/hbm.25961>